SIAM J. APPL. MATH.
Vol. 64, No. 6, pp. 1907–1932

NUMERICAL SOLUTION OF THE CAUCHY PROBLEM FOR THE STATIONARY SCHRÖDINGER EQUATION USING FADDEEV'S GREEN FUNCTION*

MASARU IKEHATA† AND SAMULI SILTANEN‡

Abstract. Numerical solution of the Cauchy problem for the stationary Schrödinger equation in a bounded two-dimensional domain is discussed. The solution algorithm is based on the properties of Faddeev's Green function. Numerical examples with computer-simulated data are presented, including an application to the inverse potential problem of electrocardiography.

Key words. Cauchy problem, stationary Schrödinger equation, exponentially growing solution, Faddeev's Green function, electrocardiography

AMS subject classifications. 15A15, 15A09, 15A23, 65N21

DOI. 10.1137/S0036139903424916

1. Introduction.

The Cauchy problem for an elliptic equation is an ill-posed problem appearing in engineering, medical imaging, and geophysics. One important application is to recover the stationary temperature inside a given body from the temperature and heat flux on the boundary of the body. Another application is the inverse problem of electrocardiography, or determination of electric voltage potential on the surface of the heart from measurements on the skin.

We consider the Cauchy problem for the stationary Schrödinger equation. Let $n = 2, 3$ and let $\Omega \subset \mathbb{R}^n$ be a bounded connected domain with Lipschitz boundary. Let $u \in H^2(\Omega)$ satisfy

$$(-\Delta + V)u = 0 \qquad \text{in } \Omega, \tag{1}$$

where $V = V(x)$ is a known, essentially bounded and complex-valued function. We denote by ν the unit outward normal vector field to $\partial\Omega$. Given a nonempty open subset $\Gamma \subset \Omega$, the pair

$$\left(u|_\Gamma, \frac{\partial u}{\partial \nu}\Big|_\Gamma \right)$$

is called the Cauchy data of u on Γ. It is well known that the Cauchy data of u on Γ uniquely determines u in Ω. See [15] for recent uniqueness and stability results of Cauchy problems for general partial differential equations. We are interested in finding an analytic formula and a regularized algorithm for calculating the value of u at a given point in Ω.

In the case $V = 0$, (1) becomes the Laplace equation. In two dimensions the Cauchy problem for the Laplace equation is equivalent to the corresponding Cauchy

*Received by the editors March 20, 2003; accepted for publication (in revised form) October 24, 2003; published electronically August 4, 2004.

http://www.siam.org/journals/siap/64-6/42491.html

†Department of Mathematics, Faculty of Engineering, Gunma University, Kiryu 376-8515, Japan (ikehata@sv1.math.sci.gunma-u.ac.jp). The research of this author was partially supported by Grant-in-Aid for Scientific Research (C)(2) (15540154) of the Japan Society for the Promotion of Science.

‡Instrumentarium Corporation, Imaging Division, P.O. Box 20, FIN-04301 Tuusula, Finland (samuli.siltanen@iki.fi). The research of this author was supported by Grant-in-Aid for JSPS Fellows (00002757) of the Japan Society for the Promotion of Science.

problem for the Cauchy–Riemann system of equations provided Ω is simply connected. Carleman [4] gave an explicit formula for calculating the value of the solution of the Cauchy–Riemann system of equations from the Cauchy data on a part of the boundary of a domain having a special shape. In [10] Goluzin and Krylov established a generalization of the formula in the simply connected domain. We refer the reader to [1, 20, 36] for other formulae and related results in complex analysis.

In the higher-dimensional case Yarmukhamedov [34, 35] gave explicit formulae of the Carleman type for the Laplace equation for special Ω and Γ. His result covers also the case when V is a constant function [37]. For constant coefficient partial differential equations several formulae of the Carleman type are described in Tarkhanov [29]. The approach is based on the uniqueness of the Cauchy problem, or equivalently, the Runge approximation property of the governing equations. The common point of their methods is the construction of special fundamental solutions $\Phi_\tau(x, y)$ for the governing equation that depend on a large parameter τ and have the following property: for a fixed $y \in \Omega$ the Cauchy data of $\Phi_\tau(\,\cdot\,, y)$ on $\partial\Omega \setminus \Gamma$ decay as $\tau \longrightarrow \infty$. Following M. M. Lavrent'ev [19], we call those fundamental solutions Carleman functions for the governing equation, Ω and Γ. Explicit construction of Carleman functions for (1) for general Ω and Γ in three dimensions is an interesting open problem.

In [13] the first author gave a formula of the Carleman type for (1) for general V and particular Ω and Γ. Here we present its minor modification given in [14]. The set Ω is the intersection of a convex open set with the half-space $x_n > 0$, and Γ is the part of $\partial\Omega$ satisfying $x_n > 0$. Let us describe the result in the two-dimensional case. The construction of the formula is divided into three steps: first, given $y \in \Omega$, let $D \subset \Omega \cap \{x_2 < y_2\}$ be the interior of a triangle with vertex at y. Second, construct the exponentially growing solution v_τ of Sylvester and Uhlmann [28] for the Schrödinger equation

$$(-\Delta + \tilde{V})v_\tau = \chi_D e^{\tau(x_2-y_2)+i\tau x_1} \quad \text{in } \mathbb{R}^2, \tag{2}$$

where $\tilde{V}$ is the zero extension of V outside Ω. Then the restriction of v_τ to Ω satisfies the equation

$$(-\Delta + V)v_\tau = \chi_D e^{\tau(x_2-y_2)+i\tau x_1} \quad \text{in } \Omega. \tag{3}$$

Third, establish the following asymptotic behavior as $\tau \to \infty$:

$$\int_D e^{\tau(x_2-y_2)+i\tau x_1} u(x)dx \sim \frac{C_D}{2\tau^2} e^{i\tau y_1} u(y), \tag{4}$$

where C_D is a nonzero constant. A combination of (3) and (4) yields the following formula for the solution u of (1):

$$u(y) = \lim_{\tau\to\infty} u_\tau(y), \tag{5}$$

where

$$u_\tau(y) := \frac{2\tau^2 e^{-i\tau y_1}}{C_D} \int_\Gamma \left(\frac{\partial u}{\partial \nu} v_\tau - \frac{\partial v_\tau}{\partial \nu} u \right) d\sigma(x). \tag{6}$$

The construction of exponentially growing solutions is based on the properties of Faddeev's Green function [8],

$$G_\zeta(x) := \frac{e^{i\zeta\cdot x}}{(2\pi)^2} \int_{\mathbb{R}^2} \frac{e^{ix\cdot\xi}}{|\xi|^2 + 2\zeta\cdot\xi} d\xi, \qquad \zeta \in \mathbb{C}^2 \setminus 0, \quad \zeta\cdot\zeta = 0. \tag{7}$$

Therefore one may consider (5) as a new application of G_ζ in addition to inverse boundary value problems and inverse scattering problems (see [31] for the problems).

We present a numerical implementation of (6) in dimension two. The ill-posed Cauchy problem is regularized by choosing τ small enough for the numerical computation to be robust against noise in the data. The main computational task is numerical evaluation of the exponentially growing solutions and their normal derivatives. For this we present an improvement of the algorithm for G_ζ given in [26] and write the derivatives of G_ζ in terms of itself and explicit formulae. The exponentially growing solutions and their derivatives can be computed combining the above with the algorithm introduced in [22] (a modification of the fast Lippmann–Schwinger equation solver of Vainikko [32, 24]). These algorithms have independent interest in the fields of electrical impedance tomography and inverse scattering.

We review some earlier numerical works on the Cauchy problem for the elliptic equation. The constant coefficient case has been studied by Leitão [21], Berntsson and Eldén [2], Cheng et al. [6], Kabanikhin and Karchevsky [16], and Háo and Lesnic [12]. The method of quasi reversibility proposed by Lattés and Lions [18] covers the variable coefficient case, and Klibanov and Santosa [17] gave an explicit estimate of the convergence rate. However, in the proof of the convergence, the uniqueness of the Cauchy problem is essential.

The present solution algorithm does not require uniqueness of the Cauchy problem for the convergence proof, and its implementation does not involve solution of boundary value problems. The computational effort is divided into two parts: first, evaluation of $v_\tau|_\Gamma$ and $\partial v_\tau/\partial\nu|_\Gamma$ for given y, V, Ω, and τ and, second, evaluation of u_τ for given Cauchy data. The second computation is very fast since it is essentially linear filtering of the data. The method can thus be applied to real-time monitoring of fixed targets with changing Cauchy data.

This paper is organized as follows. In section 2 we give details of the reconstruction formula. In section 3 we discuss the stability of our method when applied to noisy data. In section 4 we describe some properties of Faddeev's Green function and show how to evaluate it numerically. In section 5 we describe a numerical implementation of (6). We illustrate the algorithm in sections 6 and 7 by numerical examples using computer-simulated noisy data.

2. Background of the method. Throughout the paper we assume that Ω is the intersection of the open unit disc $B = \{x \in \mathbb{R}^2 \,|\, |x| < 1\}$ with the half-plane $\{x \in \mathbb{R}^2 \,|\, x_2 > t\}$ with $-1 < t < 1$ and that Cauchy data is given on $\Gamma = \{x \in \partial B \,|\, x_2 > t\}$. There is no loss of generality with this simplification of the geometry of Ω since any simply connected domain with a smooth boundary can be conformally mapped to the case when $t = 0$ (see Figure 2.1). However, in section 7 we will consider the case when $t \neq 0$.

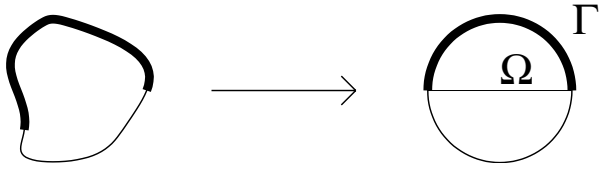

FIG. 2.1. *Conformal mapping of a domain onto the upper half of the unit disc.*

Let u be an $H^2(\Omega)$ solution of the stationary Schrödinger equation

$$-\Delta u + Vu = 0 \quad \text{in } \Omega, \tag{8}$$

where V belongs to the following class.

DEFINITION 2.1. *The potential V is admissible if V is C^2 in each component of $\Omega \setminus c$, where $c = \cup_{j=1}^{J} c_j$ with $c_j \subset \Omega$ compact, piecewise C^1 curves for which $c_i \cap c_j$ is a discrete set if $i \neq j$.*

The set D mentioned in the introduction is defined as follows.

DEFINITION 2.2. *Given $y = (y_1, y_2) \in \Omega$, let $L, p, q \in \mathbb{R}$ satisfy $0 < L \leq y_2 - t$ and*

$$-\sqrt{1-(y_2-L)^2} < y_1 + p < y_1 + q < \sqrt{1-(y_2-L)^2}. \tag{9}$$

We call the interior of the triangle with vertices

$$y = (y_1, y_2),\ y' = (y_1 + p, y_2 - L),\ y'' = (y_1 + q, y_2 - L) \tag{10}$$

a triangular patch D at y (see Figure 2.2). Although not explicitly indicated, D depends on the point y and the parameters L, p, q. D is an open subset of Ω and satisfies $D \subset \{x \,|\, x_2 < y_2\}$.

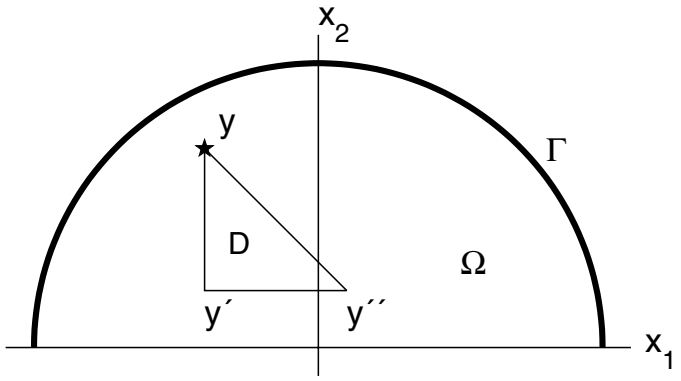

FIG. 2.2. *Geometry of the problem for $t = 0$. Domain Ω is the intersection of the unit disc with the upper half-space $x_2 > 0$. The set $\Gamma \subset \partial\Omega$ is drawn as a thick curve. The reconstruction point y is marked with a star, and one possible choice for the triangular patch D is drawn below y.*

In what follows, we take for simplicity $t = 0$.

Let χ_D denote the characteristic function of D. Let $\tilde{V}$ denote the zero extension of V outside Ω. By Sylvester and Uhlmann [28], for large $\tau \gg 1$ there exists the unique solution w_τ of the integral equation

$$\begin{aligned} w_\tau(x) + \int_{\mathbb{R}^2} g_\tau(x-z)\{\tilde{V}(z) - \chi_D(z)\} w_\tau(z) dz \\ = -\int_{\mathbb{R}^2} g_\tau(x-z)\{\tilde{V}(z) - \chi_D(z)\} dz \end{aligned} \tag{11}$$

such that for $-1 < \delta < 0$

$$\|w_\tau\|_\delta \equiv \left(\int_{\mathbb{R}^2} |w_\tau(x)|^2 (1+|x|^2)^\delta dx \right)^{\frac{1}{2}} = O\left(\frac{1}{\tau}\right). \tag{12}$$

Here g_τ is defined for any $\tau > 0$ by

$$g_\tau(x) = \frac{1}{(2\pi)^2} \int_{\mathbb{R}^2} \frac{e^{ix\cdot\xi} d\xi}{|\xi|^2 + 2\tau(\xi_1 - i\xi_2)}. \tag{13}$$

Note that g_τ satisfies $\{\Delta + 2i\tau(\partial_1 - i\partial_2)\} g_\tau(x) + \delta(x) = 0$ in $\mathbb{R}^2$.

For any $\tau > 0$ the function

$$v_\tau^0(x) = e^{\tau(x_2 - y_2)} e^{i\tau x_1}, \quad x \in \mathbb{R}^2,$$

is harmonic and has the following properties:

If $x_2 > y_2$, then $|v_\tau^0|$ is exponentially growing as $\tau \longrightarrow \infty$.

If $x_2 < y_2$, then $|v_\tau^0|$ is exponentially decaying as $\tau \longrightarrow \infty$.

We see that

$$v_\tau^0(x) g_\tau(x) = e^{-\tau y_2} G_{(\tau, -i\tau)}(x), \tag{14}$$

where $G_{(\tau,-i\tau)}$ is Faddeev's Green function (7). Then one knows that the functions $v'_\tau \equiv v_\tau^0(1 + w_\tau)$ become the solutions of the equation

$$-\Delta v'_\tau + \tilde{V} v'_\tau = \chi_D v'_\tau \quad \text{in } \mathbb{R}^2$$

and satisfy $v'_\tau \sim v_\tau^0$ as $\tau \to \infty$ in the sense that (12) holds. Define

$$v_\tau = v'_\tau|_\Omega. \tag{15}$$

Since $v'_\tau \in H^2_{\mathrm{loc}}(\mathbb{R}^2)$, v_τ is an $H^2(\Omega)$ solution of the equation

$$-\Delta v_\tau + V v_\tau = \chi_D v_\tau \quad \text{in } \Omega.$$

Now, by Theorem 2.1 of [13]

$$u(y) = \lim_{\tau\to\infty} u_\tau(y) = \lim_{\tau\to\infty} \frac{2\tau^2 e^{-i\tau y_1}}{C_D} \int_\Gamma \left(\frac{\partial u}{\partial \nu} v_\tau - \frac{\partial v_\tau}{\partial \nu} u \right) d\sigma(x), \tag{16}$$

where

$$C_D := \frac{2L(q-p)}{(L - ip)(L - iq)}. \tag{17}$$

The proof uses the estimate $\|w_\tau\|_{L^\infty(\Omega)} = O(\frac{1}{\tau})$ which comes from (2.11) of Proposition 2.3 in [27] and the well-known fact that the growth rate of $\|w_\tau\|_{H^2(\Omega)}$ with respect to τ is at most algebraic.

Note that one can give a simpler choice of v_τ appearing in (16). This is done in [14]. More precisely, for large $\tau \gg 1$ there exists the unique solution w'_τ of the integral equation

$$w'_\tau(x) + \int_{\mathbb{R}^2} g_\tau(x - z) \tilde{V}(z) w'_\tau(z) dz = \int_{\mathbb{R}^2} g_\tau(x - z) \chi_D(z) dz \tag{18}$$

such that for $-1 < \delta < 0$ we have $\|w'_\tau\|_\delta = O(1/\tau)$. Then

$$v''_\tau = v_\tau^0 w'_\tau \tag{19}$$

satisfies the equation $-\Delta v''_\tau + \tilde{V} v''_\tau = \chi_D v_\tau^0$ in $\mathbb{R}^2$. A trivial modification of the proof of Theorem 2.1 of [13] shows that (16) holds with the choice

$$v_\tau = v''_\tau|_\Omega. \tag{20}$$

In this case we use only the algebraic growth of $\|w'_\tau\|_{H^2(\Omega)}$ with respect to τ. Hereafter we consider v_τ given by (20) and not by (15).

3. Stability of the method. In this section we consider the case when the Cauchy data of u on Γ contains noise. Let $M > 0$ satisfy

$$\|V\|_{L^\infty(\Omega)} \leq M.$$

Given $y \in \Omega$ choose a triangular patch D at y according to Definition 2.2. Fix $\delta \in]-1, 0[$. Using a perturbation argument, (2.7) in Proposition 2.1 in [23], and the argument made for the proof of (2.53) in Lemma 2.11 of [23], one obtains the unique solvability of (18). More precisely, there exist positive constants $C_1(M)$ and $C_2(M)$ (independent of y and D) such that for $\tau > C_1(M)$ the equation (18) has a unique solution w'_τ satisfying the estimate

$$\tau\|w'_\tau\|_\delta + \|\nabla w'_\tau\|_\delta + \tau^{-1}\sum_{i,j=1}^{2}\|\partial_i\partial_j w'_\tau\|_\delta \leq C_2(M). \tag{21}$$

For v_τ given by (20) and $(f, g) \in L^2(\Gamma) \times L^2(\Gamma)$ define

$$S_\tau(f, g)(y) = \frac{2\tau^2 e^{-i\tau y_1}}{C_D}\int_\Gamma \left(gv_\tau - \frac{\partial v_\tau}{\partial \nu} f\right) d\sigma.$$

Let $E = (E_1, E_2) \in L^2(\Gamma) \times L^2(\Gamma)$ be additive noise on the Cauchy data on Γ. Denote $\|E\| = (\|E_1\|^2_{L^2(\Gamma)} + \|E_2\|^2_{L^2(\Gamma)})^{1/2}$.

The problem is to calculate an approximate value of $u(y)$ from

$$S_\tau\left(u|_\Gamma + E_1, \left.\frac{\partial u}{\partial \nu}\right|_\Gamma + E_2\right)(y)$$

with $\tau > C_1(M)$ when $\|E\|$ is small. One cannot choose extremely large τ since such a selection enlarges the effect of noise. The suitable choice of τ is just the problem of regularizing the formula (16).

In order to describe a result quantitatively and show the effect of the choice of D we prepare two lemmas.

LEMMA 3.1. *Assume that u belongs to the space of Hölder continuous functions $C^{0,\theta}(\overline{D})$ with $0 < \theta \leq 1$. Then for all $\tau > 0$ we have*

$$\begin{aligned}&\left|\tau^2 e^{-\tau(y_2+iy_1)}\int_D u(x)e^{\tau(x_2+ix_1)}dx - \frac{C_D}{2}u(y)\right| \\ &\leq \frac{q-p}{L}\|u\|_{C^{0,\theta}(\overline{D})}\left\{(\tau L+1)e^{-\tau L} + \left(\frac{\operatorname{diam} D}{L}\right)^\theta \frac{C_\theta}{\tau^\theta}\right\},\end{aligned} \tag{22}$$

where C_θ is a positive constant depending only on θ, and q, p, L are as in Definition 2.2.

Proof. See [13, Lemma 2]. □

LEMMA 3.2. *Let $0 < \epsilon < 1$ and y satisfy $y_2 > \epsilon$. There exists such a positive constant $C_{M,\epsilon}$ depending on M and ϵ that for any $u \in H^2(\Omega)$ and v_τ with $\tau > C_1(M)$ given by (20) the following estimate holds:*

$$\left|\tau^2 e^{-i\tau y_1}\int_{\partial\Omega\setminus\Gamma}\left(\frac{\partial u}{\partial \nu}v_\tau - \frac{\partial v_\tau}{\partial \nu}u\right)d\sigma\right| \leq C_{M,\epsilon}\|u\|_{H^2(\Omega)}\tau^3 e^{-\frac{\tau\epsilon}{2}}. \tag{23}$$

Proof. Using (19), (20), (21), and the estimate $|e^{\tau(x_2-y_2)}| \le e^{-\tau\varepsilon/2}$ for $x \in \Omega_\varepsilon$ we obtain

$$\|v_\tau\|_{H^2(\Omega_\epsilon)} \le C'_M \tau e^{-\frac{\tau\epsilon}{2}}, \tag{24}$$

where $\Omega_\epsilon = \{x \in \Omega \,|\, 0 < x_2 < \epsilon/2\}$ and C'_M is a positive constant independent of ϵ. Since $\partial\Omega_\epsilon$ is Lipschitz, we have the following consequence of a general trace theorem [11]: for any $\phi \in H^2(\Omega_\varepsilon)$ we have

$$\|\nabla\phi\|_{L^2(\partial\Omega_\varepsilon)} + \|\phi\|_{L^2(\partial\Omega_\varepsilon)} \le C_\varepsilon \|\phi\|_{H^2(\Omega_\varepsilon)}. \tag{25}$$

Combining (24) and (25) yields (23). ∎

Now we discuss the problem mentioned above. Integration by parts yields

$$\tau^2 e^{-i\tau y_1} \int_\Gamma \left(\frac{\partial u}{\partial \nu} v_\tau - \frac{\partial v_\tau}{\partial \nu} u \right) d\sigma = \tau^2 e^{-\tau(y_2+iy_1)} \int_D u(x) e^{\tau(x_2+ix_1)} dx + \tau^2 e^{-i\tau y_1} \int_{\partial\Omega\setminus\Gamma} \left(\frac{\partial u}{\partial \nu} v_\tau - \frac{\partial v_\tau}{\partial \nu} u \right) d\sigma.$$

Recalling (6), we rewrite

$$\frac{C_D}{2} u_\tau(y) = \frac{C_D}{2} u(y) + \left\{ \tau^2 e^{-\tau(y_2+iy_1)} \int_D u(x) e^{\tau(x_2+ix_1)} dx - \frac{C_D}{2} u(y) \right\} + \tau^2 e^{-i\tau y_1} \int_{\partial\Omega\setminus\Gamma} \left(\frac{\partial u}{\partial \nu} v_\tau - \frac{\partial v_\tau}{\partial \nu} u \right) d\sigma.$$

This together with (22) and (23) yields

$$|u_\tau(y) - u(y)| \frac{|C_D|}{2} \le \frac{q-p}{L} \|u\|_{C^{0,\theta}(\overline{D})} \left\{ (\tau L + 1) e^{-\tau L} + \left(\frac{\operatorname{diam} D}{L} \right)^\theta \frac{C_\theta}{\tau^\theta} \right\} + C_{M,\epsilon} \|u\|_{H^2(\Omega)} \tau^3 e^{-\frac{\tau\epsilon}{2}}. \tag{26}$$

This is an error estimate of the formula (16), and the order of the convergence is $O(\tau^{-\theta})$ as $\tau \longrightarrow \infty$.

Write

$$S_\tau \left(u|_\Gamma + E_1, \left. \frac{\partial u}{\partial \nu} \right|_\Gamma + E_2 \right)(y) = u_\tau(y) + S_\tau(E_1, E_2)(y).$$

From (17) one has

$$|C_D| = \frac{2L(q-p)}{\sqrt{L^2+p^2}\sqrt{L^2+q^2}} \le 2. \tag{27}$$

Recalling (19) and (20), from (21) we have

$$\|v_\tau\|_{H^2(\Omega)} \le C'_M \tau e^{\tau(1-y_2)}, \qquad \tau > C_1(M), \tag{28}$$

where C'_M is a positive constant. Using (27), (28), and the trace theorem we see that there exists a positive constant C''_M such that

$$\left| S_\tau \left(u|_\Gamma + E_1, \left. \frac{\partial u}{\partial \nu} \right|_\Gamma + E_2 \right)(y) - u_\tau(y) \right| \frac{|C_D|}{2} \le C''_M \|E\| \tau^3 e^{\tau(1-y_2)}. \tag{29}$$

Let $A > 0$ satisfy

$$\|u\|_{H^2(\Omega)} \leq A. \tag{30}$$

By the Sobolev imbedding theorem, one can choose a positive constant C'_θ depending on $0 < \theta < 1$ such that for all $v \in H^2(\Omega)$

$$\|v\|_{C^{0,\theta}(\overline{\Omega})} \leq C'_\theta \|v\|_{H^2(\Omega)}. \tag{31}$$

Now from (26), (29), (30), and (31) we obtain

$$\begin{aligned}
&\sup_{\|E\| \leq \eta} \left| S_\tau \left(u|_\Gamma + E_1, \left. \frac{\partial u}{\partial \nu} \right|_\Gamma + E_2 \right)(y) - u(y) \right| |C_D| \\
&\quad \leq \frac{q-p}{L} C'_\theta A \left\{ (\tau L + 1) e^{-\tau L} + \left(\frac{\operatorname{diam} D}{L} \right)^\theta \frac{C_\theta}{\tau^\theta} \right\} \\
&\quad + C_{M,\epsilon} A \tau^3 e^{-\frac{\tau \epsilon}{2}} + C''_M \eta \tau^3 e^{\tau(1-y_2)}.
\end{aligned} \tag{32}$$

The last term of this right-hand side estimates the speed of enlarging the effect of noise. We choose a suitable $\tau > C_1(M)$ depending on η in such a way that for this τ the right-hand side converges to zero as $\eta \longrightarrow 0$. There should be several choices of τ. Here we ignore the exponential decaying terms in the right-hand side of (32) and consider minimizing the remaining term $f(\tau; \eta)$ with respect to $\tau > C_1(M)$:

$$f(\tau; \eta) = \frac{\alpha}{\tau^\theta} + \beta \eta \tau^3 e^{\tau(1-y_2)},$$

where

$$\alpha = \frac{q-p}{L} C'_\theta A \left(\frac{\operatorname{diam} D}{L} \right)^\theta C_\theta; \qquad \beta = C''_M.$$

Since $\lim_{\tau \longrightarrow 0} f(\tau; \eta) = \infty$ and $\lim_{\tau \longrightarrow \infty} f(\tau; \eta) = \infty$, $f(\tau; \eta)$ attains its minimum value in a point in the interval $]0, \infty[$. The point has to satisfy the equation $f'(\tau; \eta) = 0$. This is equivalent to the equation

$$\tau^{\theta+3} \{3 + (1 - y_2)\tau\} e^{\tau(1-y_2)} = \frac{\alpha \theta}{\beta \eta}. \tag{33}$$

This equation has a unique positive solution and can be written as

$$\tau = \tau \left(\frac{\alpha \theta}{\beta \eta}, y_2 \right) = \frac{1}{1 - y_2} w \left(\frac{\alpha \theta}{\beta \eta} (1 - y_2)^{\theta+3} \right),$$

where $w = w(s), s > 0$, is the unique positive solution of the equation

$$w^{\theta+3}(3 + w) e^w = s. \tag{34}$$

If $\tau(\alpha\beta/\beta\eta, y_2) \leq C_1(M)$, then $f(\tau; \eta)$ does not attain its greatest lower bound in the interval $]C_1(M), \infty[$. So we assume that the magnitude of the noise η satisfies

$$\tau \left(\frac{\alpha \theta}{\beta \eta}, y_2 \right) > C_1(M).$$

This is equivalent to the inequality

$$C_1(M)^{\theta+3}\{3+(1-y_2)C_1(M)\}e^{C_1(M)(1-y_2)} < \frac{\alpha\theta}{\beta\eta},$$

that is,

$$\eta < \frac{\alpha\theta C_1(M)^{-(\theta+3)}e^{-C_1(M)(1-y_2)}}{\beta\{3+(1-y_2)C_1(M)\}}. \tag{35}$$

From (33) we have

$$\min_{\tau>C_1(M)} f(\tau;\eta) = f\left(\tau\left(\frac{\alpha\theta}{\beta\eta},y_2\right);\eta\right) = \frac{\alpha}{\tau(\frac{\alpha\theta}{\beta\eta},y_2)^{\theta}}\left\{1+\frac{\theta}{3+(1-y_2)\tau(\frac{\alpha\theta}{\beta\eta},y_2)}\right\}; \tag{36}$$

for $\tau = \tau(\alpha\theta/\beta\eta, y_2)$,

$$e^{-\tau L} = \left(\frac{\beta\eta}{\alpha\theta}\right)^{\frac{L}{1-y_2}}\{\tau^{\theta+3}(3+(1-y_2)\tau)\}^{\frac{L}{1-y_2}}, \tag{37}$$

$$e^{-\tau\epsilon/2} = \left(\frac{\beta\eta}{\alpha\theta}\right)^{\frac{\epsilon/2}{1-y_2}}\{\tau^{\theta+3}(3+(1-y_2)\tau)\}^{\frac{\epsilon/2}{1-y_2}}. \tag{38}$$

It is easy to see that, from (34), we have $w(s)\sim\log s$ as $s\longrightarrow\infty$, and one concludes that, as $\eta\longrightarrow 0$,

$$\tau\left(\frac{\alpha\theta}{\beta\eta},y_2\right) \sim \frac{1}{1-y_2}\log\left\{\frac{\alpha\theta}{\beta\eta}(1-y_2)^{\theta+3}\right\}. \tag{39}$$

Therefore the order of blowing up of τ is $|\log\eta|$ as $\eta\longrightarrow 0$. Moreover, from (34) one knows that $w(s)\sim(s/3)^{1/(\theta+3)}$ as $s\longrightarrow 0$. Then, for fixed η that satisfies the condition

$$\eta < \min_{y_2>\epsilon}\frac{\alpha\theta C_1(M)^{-(\theta+3)}e^{-C_1(M)(1-y_2)}}{\beta\{3+(1-y_2)C_1(M)\}} = \frac{\alpha\theta C_1(M)^{-(\theta+3)}e^{-C_1(M)(1-\epsilon)}}{\beta\{3+(1-\epsilon)C_1(M)\}},$$

we obtain, as $y_2\longrightarrow 1$,

$$\tau\left(\frac{\alpha\theta}{\beta\eta},y_2\right)\sim\left(\frac{\alpha\theta}{3\beta\eta}\right)^{\frac{1}{\theta+3}}.$$

Note that from (36), (37), (38), and (39) we obtain, for $\tau=\tau(\alpha\theta/\beta\eta,y_2)$,

$$\sup_{\|E\|\le\eta}\left|S_\tau\left(u|_\Gamma+E_1,\left.\frac{\partial u}{\partial\nu}\right|_\Gamma+E_2\right)(y)-u(y)\right||C_D| = O(|\log\eta|^{-\theta})$$

as $\eta\longrightarrow 0$. This is a regularized formula of (16).

It should be noted that the above type of argument for choosing τ is due to Lavrent'ev [19]. Therein he gave a regularization of Carleman's original formula.

We remark also that the conformal mapping depicted in Figure 2.1 deforms the potential in such a way that the bound M can become very large. This in turn makes the error estimates worse and can have an impact on the quality of the numerical solution.

4. Faddeev's Green function.

4.1. Definitions and basic properties. Consider the differential operator $\Delta_\zeta := \Delta + 2i\zeta \cdot \nabla$ with $\zeta \in \mathbb{C}^2 \setminus 0$ satisfying $\zeta \cdot \zeta = 0$. Any such ζ can be written in the form $\zeta = (k, \pm ik)$ for some $k \in \mathbb{C} \setminus 0$. We consider fundamental solutions

$$g_k^\pm(x) = \frac{1}{(2\pi)^2} \int_{\mathbb{R}^2} \frac{e^{ix\cdot\xi}}{|\xi|^2 + 2k(\xi_1 \pm i\xi_2)} d\xi, \qquad k \in \mathbb{C} \setminus 0, \tag{40}$$

satisfying

$$-\Delta_{(k,\pm ik)} g_k^\pm(x) = \Big(-\Delta - 2ik\Big(\frac{\partial}{\partial x_1} \pm i\frac{\partial}{\partial x_2}\Big)\Big) g_k^\pm(x) = \delta(x). \tag{41}$$

Then Faddeev's Green function (7) takes the form

$$G_{(k,\pm ik)}(x) = e^{ik(x_1 \pm ix_2)} g_k^\pm(x), \qquad k \in \mathbb{C} \setminus 0. \tag{42}$$

We see from (40) that the two types of fundamental solutions are related by

$$g_k^-(x) = \overline{g_{\bar k}^+(-x)}. \tag{43}$$

Moreover, coordinate changes in (40) give the following symmetries:

$$g_k^+(x) = g_1^+(kx), \qquad g_k^+(x) = \overline{g_{\bar k}^+(-\bar x)}, \qquad g_k^+(x) = e_{-k}(x)\overline{g_k^+(x)}, \tag{44}$$

where $e_{-k}(x) = \exp(-i(kx + \bar k \bar x))$. It is easy to see from (13), (43), and (44) that

$$g_\tau(x) = g_\tau^-(x) = \overline{g_\tau^+(-x)} = \overline{g_1^+(-\tau x)}. \tag{45}$$

4.2. Numerical evaluation of g_1^+. We improve here the algorithm for g_1^+ given in [25, 26]. Divide the plane into disjoint regions $D_1, \dots, D_7$ as in Figure 4.1. We describe how to numerically evaluate $g_1^+(x)$ accurately in each region.

In region $D_1 = \{|x| \le R_1\}$ with $R_1 = 5.5$ we use formulae (3.10) and (3.12) of [3]:

$$g_1^+(x) = -\frac{e^{-ix}}{4\pi}\Big(2\gamma + \log|x|^2 + \sum_{n=1}^{\infty} \frac{(ix)^n + (-i\bar x)^n}{nn!}\Big), \tag{46}$$

where $\gamma \approx 0.577215665$ is the Euler–Mascheroni constant. The infinite sum in (46) is truncated at $n = 23$.

In region D_3 we use formula (82) of [25]:

$$g_1(x) = \frac{e^{-ix_1}}{2\pi} \mathrm{Re}\left[-e^{ix_1} \sum_{j=0}^{N} \frac{j!}{(ix)^{j+1}} + \frac{(N+1)! e^{ix_1}}{(-x)^{N+1}} \int_0^\infty \frac{e^{-t(x_1+ix_2)}}{(t-i)^{N+2}} dt \right]. \tag{47}$$

We use $N = 6$ and implement the one-dimensional integration of the exponentially decaying integrand with Gaussian quadrature.

For region D_2 we modify (47) using residue calculus:

$$\int_0^\infty \frac{e^{-ix_2 t - x_1 t}}{(t-i)^{N+2}} dt = (1+i) \int_0^\infty \frac{e^{-is(x_2+x_1) + s(x_2 - x_1)}}{(s + is - i)^{N+2}} ds. \tag{48}$$

This modification ensures exponential decay of the integrand.

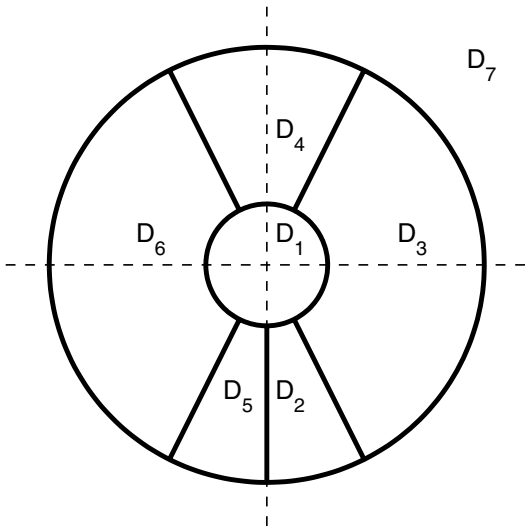

FIG. 4.1. *Computational regions $D_1, \dots, D_7$ dividing the plane into disjoint parts. The radii of the two circles are $R_1 = 5.5$ and $R_2 = 25$. The slopes of the skew lines dividing regions are either 2 or -2. It is irrelevant for the algorithm how the boundary points are divided between the regions.*

For region D_4 we modify (47) using residue calculus:

$$\int_0^\infty \frac{e^{-ix_2t-x_1t}}{(t-i)^{N+2}}dt = -i\int_0^\infty \frac{e^{-x_2s+ix_1s}}{(-is-i)^{N+2}}ds. \tag{49}$$

Again, the modified integrand decays exponentially.

For regions D_5 and D_6 we use the reflectional symmetry

$$g_1^+(-x_1, x_2) = \overline{g_1^+(x_1, x_2)} \tag{50}$$

and the algorithms for reflected regions D_2 and D_3 described above.

In region $D_7 = \{|x| \geq R_2\}$ with $R_2 = 25$ we set $N = 9$ and ignore the term with the integral in (47).

Let us comment on the choice of the radii R_1, R_2. The choice of R_1 is a trade-off: if R_1 is small, then only a few terms are needed in the truncated power series (46) to achieve desired accuracy, but on the other hand, the numerical integrations in formulae (47), (48), and (49) require many quadrature points to achieve the same accuracy. The choice $R_1 = 5.5$ gives a good balance but is not proven to be optimal. For radii $R_1 > 1$ formula (46) leads to faster computation and less memory consumption than the previous approach based on the Poisson kernel used in [25, 26]. The choice of R_2 is a similar trade-off between accuracy and computational speed.

4.3. Derivatives. As shown in [25], we can write derivatives of $g_k^\pm$ as follows.

LEMMA 4.1. *Define the functions $g_k^\pm(x)$ by (40) for $k \in \mathbb{C} \setminus 0$. Then*

$$\frac{\partial g_k^+}{\partial x_1}(x) = -\frac{1}{4\pi x} - \frac{e_{-k}(x)}{4\pi \bar{x}} - ikg_k^+(x), \tag{51}$$

$$\frac{\partial g_k^+}{\partial x_2}(x) = +\frac{1}{4\pi i x} - \frac{e_{-k}(x)}{4\pi i \bar{x}} + kg_k^+(x), \tag{52}$$

$$\frac{\partial g_k^-}{\partial x_1}(x) = -\frac{1}{4\pi\bar{x}} - \frac{e_{-\bar{k}}(x)}{4\pi x} - ikg_k^-(x), \tag{53}$$

$$\frac{\partial g_k^-}{\partial x_2}(x) = -\frac{1}{4\pi i\bar{x}} + \frac{e_{-\bar{k}}(x)}{4\pi ix} - kg_k^-(x), \tag{54}$$

where $e_{-k}(x) = \exp(-i(kx + \bar{k}\bar{x}))$, $x = x_1 + ix_2$, *and* $\bar{x} = x_1 - ix_2$.

Proof. By (43) and (44) it is enough to consider g_1^- and apply the chain rule.

Denote $\partial = (\partial/\partial x_1 - i\partial/\partial x_2)/2$. Let us compute $\partial g_1^-(x)$. By (40) we have

$$\partial g_1^-(x) = \frac{i}{2}\frac{1}{(2\pi)^2}\int_{\mathbb{R}^2}\frac{e^{ix\cdot\xi}}{\xi_1 + i\xi_2 + 2}d\xi = \frac{ie^{-2ix_1}}{2(2\pi)^2}\int_{\mathbb{R}^2}\frac{e^{ix\cdot\xi}}{\xi_1 + i\xi_2}d\xi. \tag{55}$$

Furthermore,

$$\frac{2}{i}\frac{1}{(2\pi)^2}\int_{\mathbb{R}^2}\frac{e^{ix\cdot\xi}}{\xi_1 + i\xi_2}d\xi = \frac{1}{\pi(x_1 + ix_2)}. \tag{56}$$

Combining (55) and (56) we get

$$\partial g_1^-(x) = -\frac{e^{-i2x_1}}{4\pi(x_1 + ix_2)}. \tag{57}$$

Next we determine $\bar{\partial} g_1^-(x)$. Combining (57) and (44) gives

$$-\frac{e^{i2x_1}}{4\pi(x_1 - ix_2)} = \overline{\partial g_1^-(x)} = \bar{\partial}\,\overline{g_1^-(x)} = \bar{\partial}e^{i(x+\bar{x})}g_1^-(x) = ie^{i2x_1}g_1^-(x) + e^{i2x_1}\bar{\partial}g_1^-(x),$$

and we have

$$\bar{\partial}g_1^-(x) = -\frac{1}{4\pi(x_1 - ix_2)} - ig_1^-(x). \tag{58}$$

Now formulae (57) and (58) yield the claim for $\tau = 1$ since $\partial_1 g_1^- = \partial g_1^- + \bar{\partial}g_1^-$ and $\partial_2 g_1^- = -i(\bar{\partial}g_1^- - \partial g_1^-)$. ∎

We remark that with formulae (51)–(54) any derivatives of Faddeev's Green functions can be written in terms of the Green functions themselves and explicit expressions. For instance,

$$\bar{\partial}G_{(\tau,-i\tau)}(x) = \bar{\partial}[e^{i\tau\bar{x}}g_\tau^-(x)] = e^{i\tau\bar{x}}[i\tau g_\tau^-(x) + \bar{\partial}g_\tau^-(x)] = -\frac{e^{i\tau(x_1 - ix_2)}}{4\pi(x_1 - ix_2)}. \tag{59}$$

This indicates a relationship between Faddeev's Green function and Fok–Kuni's Carleman function in the complex domain [9].

5. Numerical solution of the Cauchy problem. We discuss step by step the numerical implementation of formula (6) with fixed $y \in \Omega$.

5.1. Integration on Γ. We must choose a numerical quadrature for Γ. This is a collection of points $x^{(k)} \in \Gamma$ with $k = 1, \ldots, K$ and corresponding weights $w^{(k)}$ satisfying

$$\int_\Gamma f d\sigma \approx \sum_{k=1}^{K} w^{(k)} f(x^{(k)}). \tag{60}$$

Suitable choices are, e.g., Simpson's rule or Gaussian quadrature.

5.2. Discussion of data. We must evaluate the Cauchy data $u|_\Gamma$ and $\frac{\partial u}{\partial \nu}|_\Gamma$ on the quadrature points $x^{(k)} \in \Gamma$. How this can be done depends on the way the data are given in a particular application. We discuss here one possibility for evaluating the trace; the normal derivative can be treated similarly.

Assume that our knowledge of $u|_\Gamma$ is a finite collection of noisy point samples:

$$m_j := u(\tilde{z}^{(j)}) + \varepsilon_j, \qquad \tilde{z}^{(j)} \in \Gamma, \quad j = 1, \dots, J_0, \tag{61}$$

where ε_j for $j = 1, \dots, J_0$ are independent Gaussian, real-valued, zero-mean random variables with standard deviation $\sigma > 0$.

Define $z^{(k)} = (\cos\theta_k, \sin\theta_k) \in \Gamma$ with $\theta_k = (k-1)\pi/(J-1)$ with $k = 1, \dots, J$ and $J \geq J_0$. Assume that the data points $\tilde{z}^{(j)}$ are included in the evaluation points:

$$\tilde{z}^{(j)} = z^{(k_j)}, \qquad j = 1, \dots, J_0, \quad 1 \leq k_j \leq J. \tag{62}$$

Next we approximate $u(z^{(k)})$ under the a priori assumption that u is smooth.

Denote by $U = [U_1, \dots, U_J]^T = [u(z^{(1)}), \dots, u(z^{(J)})]^T$ the unknown values and by $m = [m_1, \dots, m_J]^T$ the measured data. We use Tikhonov regularization [30] with second derivative penalty. That is, we solve the optimization problem

$$\hat{U} := \arg \min_U \{\|\mathcal{R}U - m\|_2^2 + \alpha \|\mathcal{D}U\|_2^2\}. \tag{63}$$

The first term in the penalty functional (63) describes how well U fits the data m. The matrix $\mathcal{R}$ implements (62): each row of $\mathcal{R}$ has all zeros except the entry 1 in the k_jth column. The second term in (63) expresses our a priori knowledge on u: we know that u is smooth, so we take the matrix $\mathcal{D} : \mathbb{R}^J \to \mathbb{R}^{J-2}$ to be the second-order difference matrix

$$\mathcal{D}(U)_k = \frac{1}{(\Delta\theta)^2}(U_{k+1} - 2U_k + U_{k-1}), \qquad k = 2, \dots, J-1.$$

The parameter $\alpha > 0$ is the regularization parameter: the greater α is, the stronger we require smoothness from the reconstruction. It is practical to write (63) in the stacked form as explained by Varah [33]:

$$\begin{bmatrix} \mathcal{R} \\ \sqrt{\alpha}\mathcal{D} \end{bmatrix} U = \begin{bmatrix} m \\ 0 \end{bmatrix}. \tag{64}$$

The regularized solution $\hat{U}$ is the least squares solution of (64).

Finally, we interpolate the values $u(x^{(k)})$ at the quadrature points in (60) with spline interpolation from the recovered values $u(z^{(k)})$. Under the smoothness assumption this does not produce significant error.

5.3. Choosing the triangle D. We need a systematic choice for $D = D(y)$. The analysis in section 3 suggests the following:

1. Better results are expected in the domain $y_2 \geq 1/2$ if one chooses $L = y_2$. This is because $L \geq 1 - y_2$ and the convergence rate of (37) is better than Hölder.
2. The constant $|C_D|$ should be as large as possible because the inverse of $|C_D|$ enlarges the error (32).
3. Note that $\operatorname{diam} D/L \geq 1$ and cannot be small.

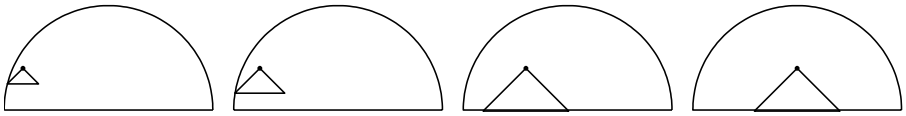

FIG. 5.1. *Triangular patches D corresponding to some y.*

We take vertices of the triangle enclosing D to be

$$(y_1, y_2), \qquad (y_1 - L, y_2 - L), \qquad (y_1 + L, y_2 - L), \tag{65}$$

with $L > 0$ taken as large as possible while still having $D \subset \Omega$. See Figure 5.1.

Now $p = -L$ and $q = L$, so

$$C_D = \frac{2L(q-p)}{(L-ip)(L-iq)} = \frac{4L^2}{L^2(1+i)(1-i)} = 2. \tag{66}$$

Note that in light of (27) this choice of C_D maximizes $|C_D|$.

5.4. Computing exponentially growing solutions. We want to evaluate the function v_τ given by (20) at the points $x^{(k)} \in \Gamma$ for $k = 1, \ldots, K$. We have $v_\tau|_\Gamma = v_\tau^0 w'_\tau|_\Gamma$ with w'_τ solving (18). In the case $V \equiv 0$, solving (18) amounts to computing a convolution. If $V \neq 0$, write (18) in the form

$$[I + g_\tau * (\tilde{V} \cdot\ )] w'_\tau = f, \tag{67}$$

where $f = g_\tau * \chi_D$. A numerical solution method for (67) is described in [22]. It is a modification of Vainikko's fast Lippmann–Schwinger solver [32, section 2]. This method is valid for potentials in the class of Definition 2.1.

Given an integer $m > 1$, the outcome of the solution algorithm is the set

$$\{w'_\tau(x^{(\ell)})\}_{\ell=1}^{M^2},$$

where the evaluation points $x^{(\ell)}$ belong to the Cartesian grid

$$\begin{aligned} &\mathcal{G}_m = \{jh \,|\, j \in \mathbb{Z}_m^2\}, \\ &\mathbb{Z}_m^2 = \{j = (j_1, j_2) \in \mathbb{Z}^2 \,|\, -2^{m-1} \le j_l < 2^{m-1},\ l = 1, 2\}, \end{aligned} \tag{68}$$

where $s > 1$ is a real number, $M = 2^m$, and $h = 2s/M$.

5.5. Computing derivatives of exponentially growing solutions. We need the values $\partial v_\tau / \partial \nu(x^{(k)})$ for $k = 1, \ldots, K$. We show that it is enough to evaluate w'_τ in addition to explicit formulae.

Take $\tau > 0$ and let w'_τ be the solution of $w'_\tau = g_\tau * \chi_D - g_\tau * (\tilde{V} w'_\tau)$. The derivatives $\partial_j w'_\tau$ for $j = 1, 2$ are given by

$$\partial_j w'_\tau = -(\partial_j g_\tau) * (\tilde{V} w'_\tau - \chi_D). \tag{69}$$

Using Lemma 4.1 we get

$$\begin{aligned}
\frac{\partial v_\tau}{\partial \nu} &= e^{-\tau y_2}\frac{\partial(e^{i\tau\bar{x}}w'_\tau)}{\partial \nu} = e^{-\tau y_2}\left[\nu_1\frac{\partial(e^{i\tau\bar{x}}w'_\tau)}{\partial x_1}+\nu_2\frac{\partial(e^{i\tau\bar{x}}w'_\tau)}{\partial x_2}\right]\\
&= e^{\tau(x_2-y_2)}e^{i\tau x_1}[i\tau\nu_1 w'_\tau+\tau\nu_2 w'_\tau-(\nu_1(\partial_1 g_\tau)+\nu_2(\partial_2 g_\tau))*(\tilde{V}w'_\tau-\chi_D)]\\
&= e^{\tau(x_2-y_2)}e^{i\tau x_1}\left[i\tau\nu_1 w'_\tau+\tau\nu_2 w'_\tau\right.\\
&\qquad -\nu_1\left(-\frac{1}{4\pi\bar{x}}-\frac{e_{-\bar{\tau}}(x)}{4\pi x}-i\tau g_\tau\right)*(\tilde{V}w'_\tau-\chi_D)\\
&\qquad \left.-\nu_2\left(-\frac{1}{4\pi i\bar{x}}+\frac{e_{-\bar{\tau}}(x)}{4\pi i x}-\tau g_\tau\right)*(\tilde{V}w'_\tau-\chi_D)\right] \qquad (70)\\
&= \frac{e^{\tau(x_2-y_2)}e^{i\tau x_1}}{4\pi}\left[\left(\nu_1\left(\frac{1}{\bar{x}}+\frac{e^{-i2\tau x_1}}{x}\right)+\nu_2\left(\frac{1}{i\bar{x}}-\frac{e^{-i2\tau x_1}}{ix}\right)\right)*(\tilde{V}w'_\tau-\chi_D)\right],
\end{aligned}$$

where we used formulae (53) and (54) and the real-valuedness of τ. Note the cancellation of four terms containing w'_τ resulting from the identity $w'_\tau = -g_\tau * (\tilde{V}w'_\tau - \chi_D)$.

5.6. Choosing τ. Theoretically, the larger $\tau > 0$ is, the closer $u_\tau(y)$ is to $u(y)$. However, too large τ leads to computations involving exponentially large numbers and numerical instability. This is even more so when the data is noisy. Thus τ must be chosen large enough for the approximation $u(y) \approx u_\tau(y)$ to be accurate enough but small enough to avoid instability. We discussed the optimal choice of τ theoretically in section 3, and in section 6 we study several choices of τ numerically.

6. Numerical results for $V \equiv 0$.

6.1. The model problem. Let $u = \mathrm{Re}((x_1 + ix_2)^4)$ be the harmonic function to be recovered from its Cauchy data on

$$\Gamma = \{x_1 + ix_2 = e^{i\theta} \,|\, 0 < \theta < \pi\} \subset \partial\Omega. \qquad (71)$$

See Figure 6.1 for a contour plot of u in the domain Ω together with plot of trace of u and plot of $\partial u/\partial\nu$.

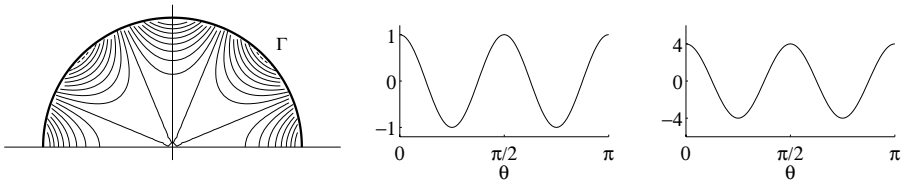

FIG. 6.1. *Left: contour plot of the harmonic function u in the domain Ω. Middle: plot of the trace $u|_\Gamma$ as function of angular parameter θ. Right: plot of normal derivative $\partial u/\partial\nu|_\Gamma$.*

6.2. Details of implementation.

Step 1*: Integration on* Γ. According to a given y, we divide Γ into three intervals:

$$0 < \theta < \tilde{\theta}, \qquad \tilde{\theta} < \theta < \pi - \tilde{\theta}, \qquad \pi - \tilde{\theta} < \theta < \pi.$$

Here $0 < \tilde{\theta} < \pi/2$ is chosen so that, roughly, the largest values of the integrand are in the interval containing $\pi/2$. We take $\tilde{\theta} = (70/360)\cdot 2\pi$. We choose K_0 Gaussian

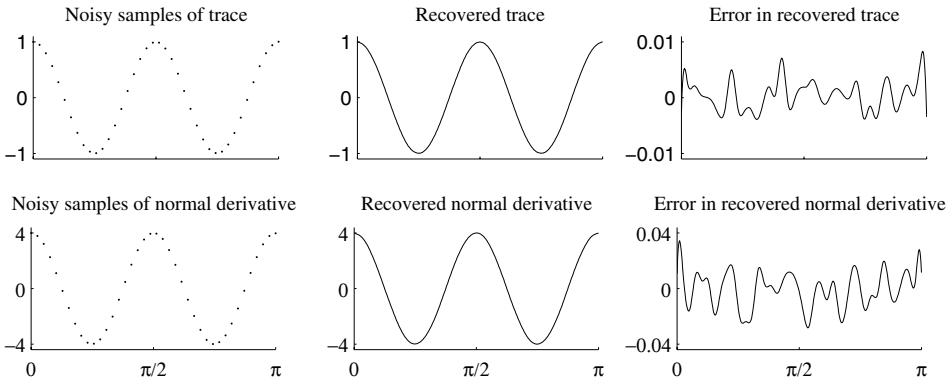

FIG. 6.2. *Simulation of noisy Cauchy data of u satisfying Laplace's equation. In each plot, the abscissa is the angular parameter θ for the curve $\Gamma = \{e^{i\theta} \,|\, 0 < \theta < \pi\}$.*

quadrature points for each interval leading to a quadrature rule of $K = 3K_0$ evaluation points for Γ.

Step 2*: Evaluation of data.* The Cauchy data of u are given by explicit formulae:

$$u|_\Gamma(\theta) = \cos 4\theta, \qquad \left.\frac{\partial u}{\partial \nu}\right|_\Gamma (\theta) = 4\cos 4\theta. \tag{72}$$

We produce simulated noisy data following the discussion in section 5.2. Set $\tilde{z}^{(j)} = (\cos\phi_j, \sin\phi_j)$ with $\phi_j = (j-1)\pi/(J_0 - 1)$ with $j = 1, \ldots, J_0 = 40$. We compute noisy samples as

$$u(\tilde{z}^{(j)}) + 0.003\,\varepsilon_j, \qquad \frac{\partial u}{\partial \nu}(\tilde{z}^{(j)}) + 0.012\,\varepsilon'_j, \tag{73}$$

where ε_j and ε'_j are normally distributed independent random numbers with standard deviation $\sigma = 1$. See Figure 6.2.

To recover the smooth data using Tikhonov regularization, we take

$$\theta_k = (k-1)\pi/(J-1), \qquad z^{(k)} = (\cos\theta_k, \sin\theta_k) \text{ for } k = 1, \ldots, J = 391.$$

The result of solving (64) with regularization parameter $\alpha = 4$ is shown in Figure 6.2. The choice of α was based on visual inspection. The L^2 norm for the noise introduced in section 3 is $E \approx 0.02$.

Step 3*: Choosing the triangle D and computing C_D.* We implement the choice given in section 5.3. For any y, we start by $L = y_2$. Generally, this leads to $D \not\subset \Omega$. Then, we replace L with $L/2$ so many times that $D \subset \Omega$. Then we replace L with $L + 0.01$ as many times as possible while still having $D \subset \Omega$. We have $C_D = 2$.

Step 4*: Evaluation of v_τ.* With fixed y and given choice of $D = D(y)$ and $\tau = \tau(y)$, we substitute $V \equiv 0$ into (18):

$$w'_\tau(x) = \int_{\mathbb{R}^2} g_\tau(x-z)\chi_D(z)dz = \int_D g_\tau(x-z)dz.$$

So we need to integrate over D to find $w'_\tau(x)$ for a given $x \in \Gamma$. We use Gaussian product quadrature with $\tilde{K}_0^2 = \tilde{K}$ evaluation points. As indicated in section 4, we have available a numerical algorithm for g_τ, so Step 4 is complete.

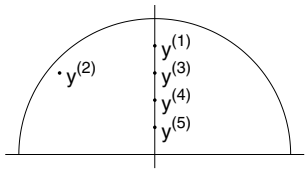

$$y^{(1)} = (0, 4/5)$$
$$y^{(2)} = (-7/10, 3/5)$$
$$y^{(3)} = (0, 3/5)$$
$$y^{(4)} = (0, 2/5)$$
$$y^{(5)} = (0, 1/5)$$

FIG. 6.3. *Special points for examining the convergence of* $u_\tau(y^{(j)})$ *to* $u(y^{(j)})$.

Step 5*: Evaluation of* $\partial v_\tau/\partial\nu$. We have $v_\tau(x) = e^{-\tau y_2}e^{i\tau\bar{x}}w'_\tau(x)$, where $w'_\tau(x) = g_\tau * \chi_D$. Compute

$$\frac{\partial v_\tau}{\partial x_1} = e^{-\tau y_2}e^{i\tau\bar{x}}\left(i\tau w'_\tau(x) + \frac{\partial w'_\tau}{\partial x_1}\right). \tag{74}$$

Further, using Lemma 4.1,

$$\frac{\partial w'_\tau}{\partial x_1} = \frac{\partial g_\tau}{\partial x_1} * \chi_D = \left(-\frac{1}{4\pi\bar{x}} - \frac{e_{-\tau}(x)}{4\pi x}\right) * \chi_D - i\tau w'_\tau. \tag{75}$$

A combination of (74) and (75) yields

$$\frac{\partial v_\tau}{\partial x_1} = -e^{-\tau y_2}e^{i\tau\bar{x}}\left(\frac{1}{4\pi\bar{x}} + \frac{e_{-\tau}(x)}{4\pi x}\right) * \chi_D. \tag{76}$$

We can compute $\partial v_\tau/\partial x_2$ in a similar fashion. Note that on Γ the normal vector ν takes the simple form $\nu(x) = (x_1, x_2)$. Thus we get

$$\left.\frac{\partial v_\tau}{\partial\nu}\right|_\Gamma = -\frac{e^{-\tau y_2}e^{i\tau\bar{x}}}{4\pi}\Big(\frac{x_1}{\bar{x}} + \frac{x_1 e_{-\tau}(x)}{x} + \frac{x_2}{i\bar{x}} - \frac{x_2 e_{-\tau}(x)}{ix}\Big) * \chi_D. \tag{77}$$

Step 6*: Choosing* τ. We want to find a suitable τ experimentally. So we will compute u_τ with τ varying in the interval $[10, 80]$. We study convergence of u_τ to u at the points $y^{(1)}, \ldots, y^{(5)}$ given in Figure 6.3. We plot $u_\tau(y^{(j)})$ for $j = 1, \ldots, 5$ as functions of τ in Figure 6.4. Note that numerical instability occurs when τ is large. This is due to finite precision of the computation and the exponential functions appearing in the reconstruction formula.

6.3. Results for ideal data. We now have a complete numerical algorithm for u_τ. Since it is numerically impossible to compute u_τ for y_2 close to zero, we choose the computational reconstruction domain as

$$\Omega' = \left\{y \in \Omega \,|\, y_2 \geq \frac{1}{8}\right\}. \tag{78}$$

We compute $u_\tau(y)$ in Ω' for $\tau = 10, 40, 70$ on a collection of 1382 evaluation points inside the upper half of the unit disc. For integration on Γ we choose $K = 360$ quadrature points, and for integration on D we take a product rule with $\tilde{K} = 25^2 = 625$ points. We show the functions u, u_{20}, u_{40}, and u_{70} in Figure 6.5.

We see that the quality of the reconstruction varies depending on y_2 and τ. In particular, we observe that each plot with fixed τ has a region of acceptable reconstruction always containing a neighborhood of the point $(0, 1)$. Furthermore, when τ grows, the region of acceptable reconstruction shrinks, but the quality of

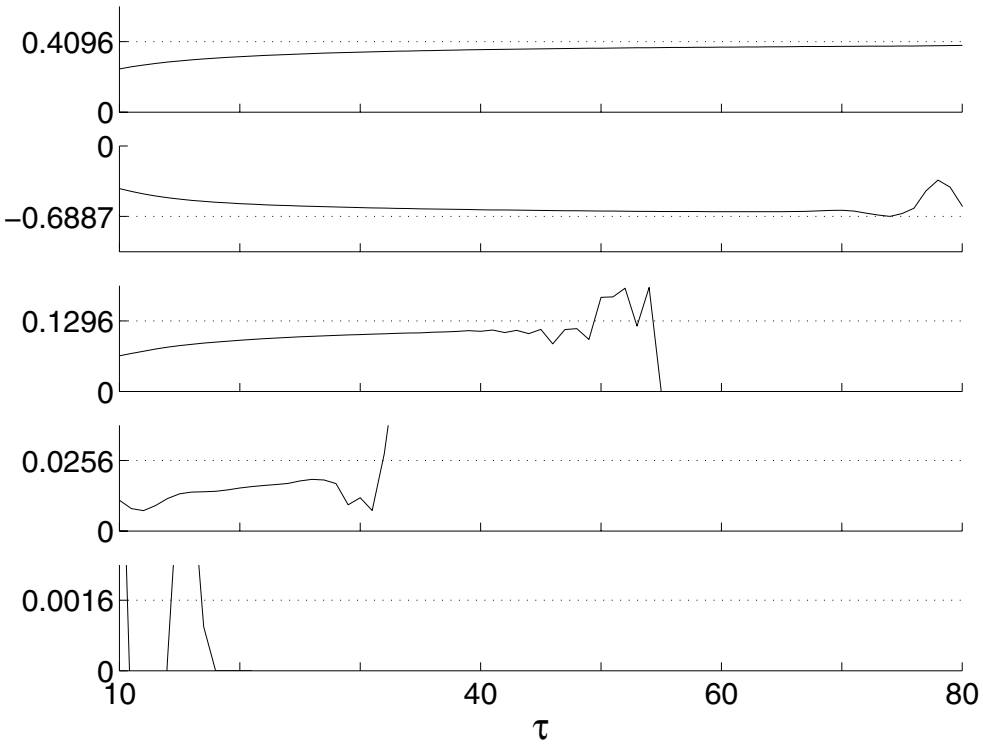

FIG. 6.4. *Convergence study for the Laplace equation. From top to bottom: plot of the real part of the function* $\tau \mapsto u_\tau(y^{(j)})$ *for* $j = 1, 2, 3, 4, 5$. *The theoretical limit values for these functions when* $\tau \to \infty$ *are marked in the plots. Note that numerical instability makes the computation inaccurate when* τ *grows. Divergence appears with smaller* τ *values for those reconstruction points that are deeper inside* Ω.

TABLE 6.1

Relative errors in u_τ *computed from ideal Cauchy data of a solution* u *to Laplace's equation. Left: relative* L^2 *errors* $E_2(t,\tau)$. *Right: relative* L^∞ *errors* $E_\infty(t,\tau)$. *In these tables, "—" stands for "greater than* 1000%." *For definitions of* E_2 *and* E_∞, *see* (79).

	$t = 1/8$	1/2	7/8
$\tau = 10$	53%	47%	45%
40	923%	16%	14%
70	—	—	9%

	$t = 1/8$	1/2	7/8
$\tau = 10$	91%	91%	33%
40	—	46%	10%
70	—	—	6%

reconstruction in the acceptable region is better than with smaller τ. For quantitative examination of this property we introduce the following norms for measuring the error of reconstructions. Given $0 < t < 1$ and $\tau > 0$, we consider the relative errors

$$E_2(t,\tau) = \frac{\|u - u_\tau\|_{L^2(\Omega_t)}}{\|u\|_{L^2(\Omega_t)}}, \qquad E_\infty(t,\tau) = \frac{\|u - u_\tau\|_{L^\infty(\Omega_t)}}{\|u\|_{L^\infty(\Omega_t)}}, \tag{79}$$

where $\Omega_t = \{y \in \Omega \,|\, y_2 > t\}$. The errors are given in Table 6.1.

For one choice of τ, the computation takes about 4 hours with MATLAB 6.5 running on a desktop PC computer with an Intel Pentium IV 2.8 GHz processor and 1 GB memory. In practical applications the collection of recovery points y and a good

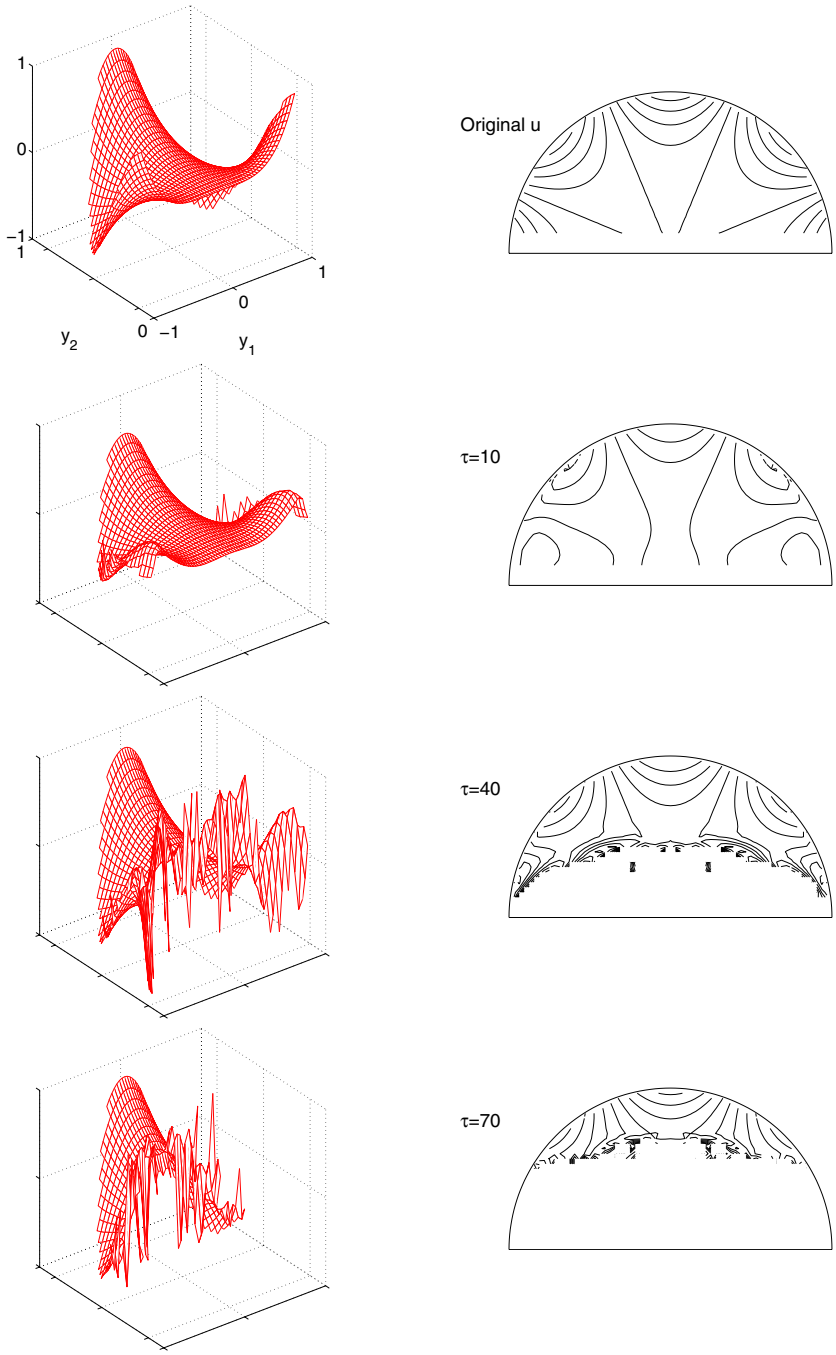

FIG. 6.5. *Results for the Laplace equation and ideal data. Top left: mesh plot of the original harmonic function u. Top right: contour plot of u. Similarly, from top to bottom, we show mesh and contour plots of the reconstructions u_{10}, u_{40}, and u_{70}. The axis limits are the same in all mesh plots, allowing easy comparison. We do not plot any function values greater than* 1 *in absolute value since numerical instability causes extremely large (incorrect) values in the reconstructions, and visualizing these values would obscure the acceptable parts of the reconstructions. Note that the greater τ is, the better the reconstruction is for points (y_1, y_2) with y_2 near* 1.

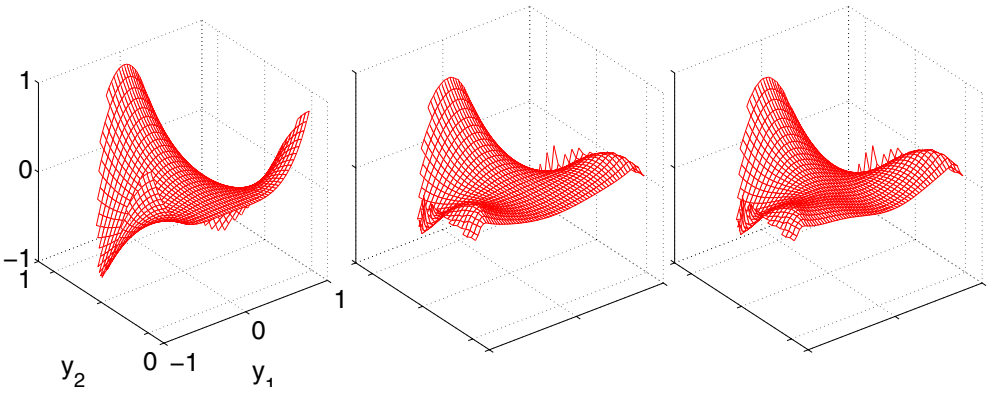

FIG. 6.6. *Results for the Laplace equation and noisy data. Left: mesh plot of the original harmonic function u. Middle: recovery of u with spatially varying τ from data with noise level* 0.3%. *Right: recovery of u with spatially varying τ from data with noise level* 0.6%.

choice for τ can be fixed. Then traces $v_\tau|_{\partial\Omega}$ and the normal derivatives $\partial v_\tau/\partial\nu|_{\partial\Omega}$ according to each y need be computed only once and saved. Then recovery of $u(y)$ with given Cauchy data takes in this case only a couple of seconds.

It can be seen in Figure 6.5 that near those parts of the boundary that are almost parallel to the y_2 axis, the quality of the reconstruction is bad. This is related to the smaller triangular patch D used there, leading to slower convergence.

6.4. Results for noisy data. We compute the functions u_7, u_{10}, and u_{12} using noisy Cauchy data. The results are similar to the nonnoisy case, the main difference being that the region of acceptable results shrinks with considerably smaller τ values. To achieve a uniform level of regularization, we choose τ as a function of y as follows:

$$\tau = \tau(y) = 6 + 6y_2^3,$$

so deep inside Ω we use a smaller value of τ, leading to less oscillation. Since the τ values used were relatively small, we did not need so many quadrature points for numerical integration. For integration on Γ we choose $K = 36$ quadrature points, and for integration on D we take a product rule with $\tilde{K} = 7^2 = 49$ points.

For the result, see the middle plot in Figure 6.6. The recovered solution has 38% relative $L^2(\Omega')$ error. To examine the robustness of our method against noise, we produce noisy data with double standard deviation in the random errors in (73). We repeat the recovery process, leading to a result having 41% relative $L^2(\Omega')$ error; see the rightmost plot in Figure 6.6. The relative difference between the two reconstructions in $L^2(\Omega')$ is only 6% although the noise level was doubled. The computation of each of the two reconstructions took 5 minutes.

7. Numerical results for $V \neq 0$. We present a two-dimensional example roughly modelling the inverse potential problem in cardiology.

7.1. The Cauchy problem in cardiology. A beating heart produces an electrical field inside the body, and the resulting voltage distribution can be measured with electrodes placed on the skin. This is called electrocardiography (ECG). The

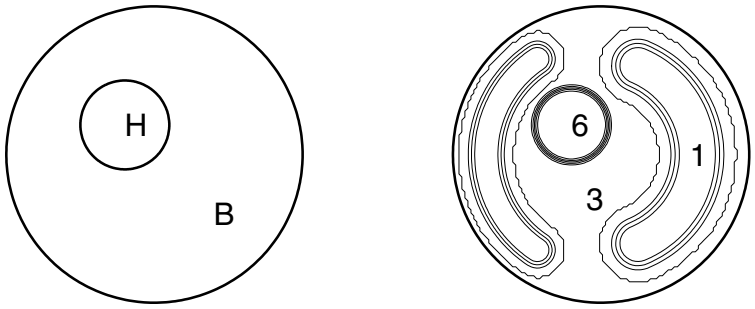

FIG. 7.1. *Left: the domain of the conductivity equation is the annulus* $\tilde{\Omega} = B \setminus H$. *Right: contour plot of the twice differentiable conductivity distribution on* B.

inverse potential problem of cardiology is of clinical interest: *given the ECG measurements and the conductivity distribution of the body, what is the voltage potential on the surface of the heart?*

We present a two-dimensional quasi-static model of the above inverse problem. Let the unit disc $B = \{x \in \mathbb{R}^2 \,|\, |x| < 1\}$ model a cross section of human thorax, and assume that the heart is located on the disc H with center at $(-0.2, 0.2) \in B$ and radius 0.3. Further, we model the electrical conductivity $\gamma : B \to \mathbb{R}$ of the body with a strictly positive $C^2(\overline{B})$ function taking value 6 in the heart, 1 in the lungs, and 3 in the background. These values approximate the tissue conductivities during perfusion. See Figure 7.1.

Electric current inside the heart results in the following boundary value problem for the electric voltage potential $\tilde{u}$ in the annulus $\tilde{\Omega} = B \setminus H$:

$$\nabla \cdot \gamma \nabla \tilde{u} = 0 \text{ in } \tilde{\Omega}, \quad \tilde{u}|_{\partial H} = f, \quad \left.\frac{\partial \tilde{u}}{\partial \nu}\right|_{\partial B} = 0, \tag{80}$$

where we assumed that the outer boundary ∂B is perfectly insulated.

We create our example by setting $f(x_1, x_2) = (x_1 + 0.5)(x_2 - 0.2)$ in (80), qualitatively resembling a voltage distribution depicted on page 386 in [7]. We solve the elliptic boundary value problem (80) with the finite element solver of MATLAB's PDE toolbox using 14848 triangles in the domain $\tilde{\Omega}$. See Figure 7.2.

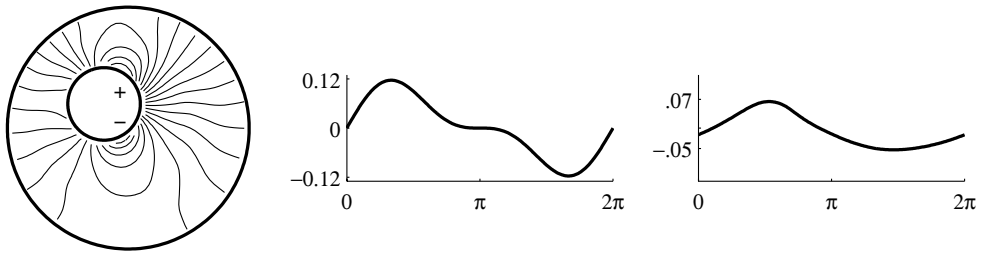

FIG. 7.2. *Left: contour plot of the solution* $\tilde{u}$ *of the conductivity equation* (80). *Middle: voltage potential* $\tilde{u}|_{\partial H}$ *on the surface of the heart as a function of the angular variable* θ *corresponding to the parametrization* $\partial H = \{(-0.2 + 0.3\cos\theta, 0.2 + 0.3\sin\theta) \in \mathbb{R}^2 \,|\, 0 \le \theta < 2\pi\}$. *Right: voltage potential* $\tilde{u}|_{\partial B}$ *as a function of the angular variable* θ *corresponding to the parametrization* $\partial B = \{(\cos\theta, \sin\theta) \in \mathbb{R}^2 \,|\, 0 \le \theta < 2\pi\}$. *Axis limits in the two plots are the same to allow quantitative comparison.*

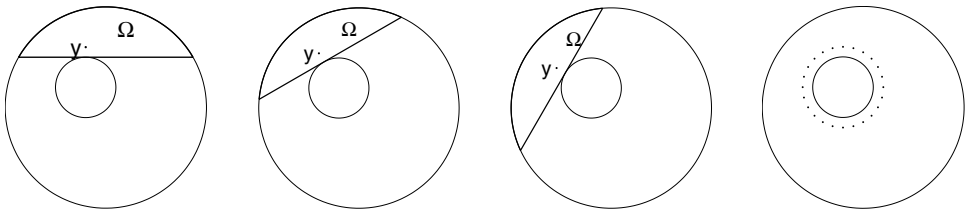

FIG. 7.3. *In the rightmost picture are* 24 *reconstruction points on the circle* S *defined in* (83) *at distance* 0.1 *from the surface of the heart. For each reconstruction point we choose a domain* Ω *that coincides after rotation with a canonical domain described in section* 2.

Application of the techniques of this paper requires transforming the conductivity equation (80) into the Schrödinger equation. Set

$$V(x) = \frac{\Delta\sqrt{\gamma(x)}}{\sqrt{\gamma(x)}}. \tag{81}$$

Since $\gamma \in C^2(\overline{B})$, we have $V \in C^0(\tilde{\Omega}) \subset L^\infty(\tilde{\Omega})$. (The norm of the particular potential we use is approximately $\|V\|_{L^\infty(\tilde{\Omega})} \approx 293$, so our example is not a small perturbation of the harmonic case.) It is straightforward to check that $u := \gamma^{1/2}\tilde{u}$ satisfies the equation

$$(-\Delta + V)u = 0 \qquad \text{in } \tilde{\Omega}. \tag{82}$$

Because $\gamma \equiv 3$ in a neighborhood of ∂B, we know the Cauchy data of u on ∂B:

$$u|_{\partial B} = \sqrt{3}\tilde{u}|_{\partial B}, \qquad \left.\frac{\partial u}{\partial \nu}\right|_{\partial B} = 0.$$

Equation (82) is valid only outside the heart. We choose a collection of computational domains Ω as shown in Figure 7.3; each of these domains coincides after rotation with a canonical domain described in section 2. We cannot choose our recovery points right at the surface of the heart because the set D would then be empty, so we choose 24 points on the circle S given by

$$S = \{(-0.2 + 0.4\cos\theta, 0.2 + 0.4\sin\theta) \in \mathbb{R}^2 \,|\, 0 \le \theta < 2\pi\}. \tag{83}$$

Thus we reconstruct the voltage at distance 0.1 from the surface of the heart. See Figure 7.3.

7.2. Details of implementation. We assume that the domain Ω is (possibly after rotation) of the canonical form with $-1 < t < 1$ described in section 2. The Neumann data of u vanish, we need only compute

$$u_\tau(y) = -\frac{2\tau^2 e^{-i\tau y_1}}{C_D} \int_\Gamma \frac{\partial v_\tau}{\partial \nu} u \, d\sigma(x). \tag{84}$$

Step 1*: Integration on* Γ. We choose K Gaussian quadrature points on Γ. There is no need to divide Γ into subintervals as done in section 6.2 since we use so small a value of τ that the integrand is roughly of the same order of magnitude throughout Γ.

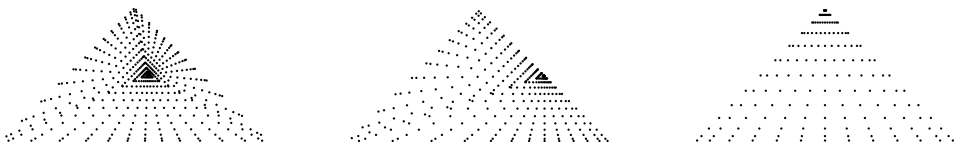

FIG. 7.4. *Product Gaussian quadratures on the triangular patch D with 13×13 points in polar coordinates. Left: the origin is inside D. Middle: the origin is on the boundary of D. Right: the origin is at the corner of D.*

Step 2*: Evaluation of data.* The experimental setup in [7] uses 24 electrodes with 2% noise level. We simulate that measurement with

$$\tilde{u}(\tilde{z}^{(j)}) + 0.0022\,\varepsilon_j,$$

where $\tilde{z}^{(j)} = (\cos\phi_j, \sin\phi_j)$ with $\phi_j = (j-1)2\pi/J_0$ with $j = 1, \ldots, J_0 = 24$ and ε_j are normally distributed independent random numbers with standard deviation 1.

We use Tikhonov regularization to recover a smooth approximation to the actual voltage. In the notation of section 5.2, we have $J_0 = 24$, $J = 144$, and $\alpha = 2$. Since we reconstruct the trace on the full circle, we include requirement of periodicity into the regularization. Relative $L^2(\partial\Omega)$ error in the reconstruction of the trace $\tilde{u}|_{\partial\Omega}$ is 0.033, and relative $L^\infty(\partial\Omega)$ error is 0.032.

Step 3*: Choosing the triangle D and computing C_D.* We take $L = 0.1$ and use the choice given in section 5.3 leading to $C_D = 2$.

Step 4*: Evaluation of v_τ.* We need to solve the Lippmann–Schwinger-type equation $[I + g_\tau * (\tilde{V}\cdot\,)]w'_\tau = f$ as explained in section 5.4. The problem is the evaluation of

$$f(x^{(\ell)}) = (g_\tau * \chi_D)(x^{(\ell)}) = \int_D g_\tau(x^{(\ell)} - y)dy, \quad \ell = 1, 2, \ldots, M^2. \tag{85}$$

Since $g_\tau(x)$ has a logarithmic singularity at $x = 0$, numerical integration in (85) becomes problematic when $x^{(\ell)}$ belongs to D or is close to the boundary ∂D. We overcome this problem by writing the integral in polar coordinates and using product Gaussian quadrature; due to the product measure $rdrd\phi$ the integrand is bounded and continuous since $\lim_{r\to 0} r\log r = 0$. We need only to go through the tedious task of writing the integration domain as a function of ϕ and $r(\phi)$. We do not bore the reader with the details of dividing the algorithm into 19 subcases and performing the necessary trigonometric calculations but instead show some resulting quadrature points in Figure 7.4.

Step 5*: Evaluation of $\partial v_\tau/\partial\nu$.* From (70) we see that the normal derivative of v_τ appearing in (84) is given by

$$\begin{aligned}
&-\frac{e^{\tau(x_2-y_2)}e^{i\tau x_1}}{4\pi}\left[\left(\nu_1\left(\frac{1}{\bar{x}} + \frac{e^{-i2\tau x_1}}{x}\right) + \nu_2\left(\frac{1}{i\bar{x}} - \frac{e^{-i2\tau x_1}}{ix}\right)\right) * \chi_D\right] \\
&+\frac{e^{\tau(x_2-y_2)}e^{i\tau x_1}}{4\pi}\left[\left(\nu_1\left(\frac{1}{\bar{x}} + \frac{e^{-i2\tau x_1}}{x}\right) + \nu_2\left(\frac{1}{i\bar{x}} - \frac{e^{-i2\tau x_1}}{ix}\right)\right) * \tilde{V}w'_\tau\right] \\
&\equiv I_1 + I_2.
\end{aligned}$$

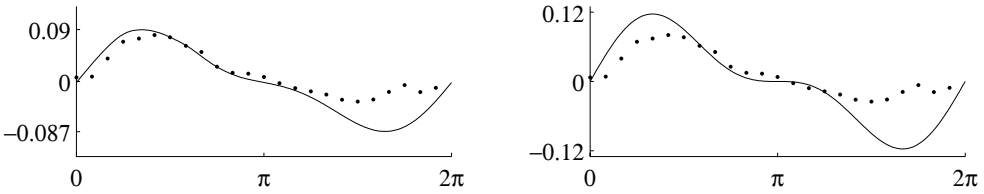

FIG. 7.5. *Left: true voltage potential at distance* 0.1 *from the boundary of the heart is plotted as a solid line. Reconstructed voltage potential values are plotted as dots. See Figure* 7.3 *for the reconstruction points. Right: true voltage potential at the boundary of the heart (solid line) and the same reconstructed voltage potentials as in the left plot (dots). The abscissa in both plots is the angular parameter of the circle around the heart.*

Note that I_2 vanishes when $V = 0$, and therefore I_2 can be seen as a correction term compensating for nonzero V. The computation of I_1 was already described for the case $V = 0$.

Given an integer $m > 1$, the outcome of Step 4 is the set $\{w'_\tau(x^{(\ell)})\}_{\ell=1}^{M^2}$, where the evaluation points $x^{(\ell)}$ belong to the grid (68). It is then natural to implement the integral in I_2 simply with the midpoint rule.

Step 6*: Choosing* τ*.* We take $\tau = 4, 6, 8, 10, 12$.

7.3. Results. To compute (84) we choose $K = 70$ for integrating over Γ, and for all integrations over D we take $\tilde{K} = 15^2 = 225$ quadrature points. We take $m = 7$, or $M = 128$ in the Lippmann–Schwinger solver. We compute u_τ with $\tau = 4, 6, 8, 10, 12$ and find that the reconstructions with $\tau > 6$ are oscillatory, and $\tau = 6$ gives a better result than $\tau = 4$. We thus choose $\tau = 6$.

The plot on the left in Figure 7.5 shows the superposition of reconstructed voltage potential $\gamma^{-1/2}u_6$ and the actual potential *on the circle* S *containing the reconstruction points*. We find that the maximum relative absolute error of the reconstruction is 86%. Diagnostically, the most interesting part of the reconstruction is the angular interval $0 \le \theta \le \pi$. In this interval, the maximum and average relative absolute errors are 25% and 10%, respectively.

However, we are interested in the voltage potential at the boundary of the heart. We simply consider our reconstruction of the voltage on S to be an approximation to the voltage on ∂H. The plot on the right in Figure 7.5 shows a comparison of these two quantities. Maximum relative absolute error in the reconstruction as compared to the voltage potential at the boundary of the heart is 1.07. In the interval $0 \le \theta \le \pi$, the maximum and average relative absolute errors are 43% and 21%, respectively.

The computation took 4 hours.

7.4. Discussion. Unlike in many works on the inverse potential problem of ECG, such as [7], we do not assume that the tissue between the skin and the surface of the heart is homogeneous. If the electric conductivity of the body is known, e.g., by electrical impedance tomography [5], our method thus allows more accurate modelling of the problem.

The worst-case performance of our algorithm is not impressive: the maximum relative error is 1.07. However, this worst error appears near the posterior surface of the heart (facing the back), which is far away from the boundary. The anterior surface of the heart (facing the chest) is diagnostically more important. Relative error on the

anterior surface, defined as $0 \leq \theta \leq \pi$ in the notation of Figure 7.2, is on average 21% and at most 43%. This result is somewhat better than the 30%–50% error reported in [7], where conductivity was taken to be constant.

Instead of quantitative reconstruction of the voltage, we might want to know the location of the maximum voltage potential on the anterior surface of the heart. The true maximum appears at $\theta_0 = 1.05$ (in radians), and the reconstruction attains its maximum at $\tilde{\theta}_0 = 1.31$. The error in the reconstructed angle is 15 degrees.

The main advantage of our method is modelling the conductivity, and the main source of error is the inherent problem that we cannot recover the voltage at the surface of the heart but slightly away from it. As mentioned in the introduction, there are other methods capable of dealing with nonconstant conductivities and additionally providing reconstruction right at the surface of the heart. However, those methods typically involve solution of boundary value problems, which is computationally intensive. Our reconstruction method is very fast after the initial computational load, and it could thus be better suited for real-time monitoring. Also, modelling the movement of a beating heart for the solution of boundary value problems is difficult, and our approach of reconstructing a little bit away from the heart might be considered an advantage.

Our tissue model assumes that the conductivity is differentiable although in reality it is discontinuous, but since many regularized electrical impedance tomography reconstructions produce a differentiable approximation to the conductivity, this is perhaps not so serious. The most obvious drawback of the presented algorithm is the two-dimensional approximation. However, the theory behind our method covers the three-dimensional case, and a similar algorithm can be designed in three dimensions. This is left for a future study.

REFERENCES

[1] L. Aizenberg, *Carleman's Formulas in Complex Analysis*, Kluwer Academic Publishers, London, 1993.

[2] F. Berntsson and L. Eldén, *Numerical solution of a Cauchy problem for the Laplace equation*, Inverse Problems, 17 (2001), pp 839–853.

[3] M. Boiti, J. P. Leon, M. Manna, and F. Pempinelli, *On a spectral transform of a KdV-like equation related to the Schrödinger operator in the plane*, Inverse Problems, 3 (1987), pp. 25–36.

[4] T. Carleman, *Les Fonctions Quasi Analytiques*, Gauthier-Villars, Paris, 1926.

[5] M. Cheney, D. Isaacson, and J. C. Newell, *Electrical impedance tomography*, SIAM Rev., 41 (1999), pp. 85–101.

[6] J. Cheng, Y. C. Hon, T. Wei, and M. Yamamoto, *Numerical computation of a Cauchy problem for Laplace equation*, ZAMM Z. Angew. Math. Mech., 81 (2001), pp. 665–674.

[7] P. Colli-Franzone, L. Guerri, S. Tentoni, C. Viganotti, S. Baruffi, S. Spaggiari, and B. Taccardi, *A mathematical procedure for solving the inverse potential problem of electrocardiography. Analysis of the time-space accuracy from in vitro experimental data*, Math. Biosci., 77 (1985), pp. 353–396.

[8] L. D. Faddeev, *Increasing solutions of the Schrödinger equation*, Sov. Phys. Dokl., 10 (1966), pp. 1033–1035.

[9] V. A. Fok and F. M. Kuni, *On the introduction of a "suppressing" function in dispersion relation*, Dokl. Akad. Nauk SSSR, 127 (1959), pp. 1195–1198 (in Russian).

[10] M. G. Goluzin and I. V. Krylov, *A generalized Carleman formula and its application to analytic continuation of functions*, Mat. Sb., 4 (1933), pp. 144–149.

[11] P. Grisvard, *Elliptic Problems in Nonsmooth Domains*, Pitman, Boston, 1985.

[12] D. N. Háo and D. Lesnic, *The Cauchy problem for Laplace's equation via the conjugate gradient method*, IMA J. Appl. Math., 65 (2000), pp. 199–217.

[13] M. Ikehata, *Exponentially growing solutions and the Cauchy problem*, Appl. Anal., 78 (2001), pp. 79–95.

[14] M. Ikehata, *The enclosure method and its applications*, in Analytic Extension Formulas and Their Applications, S. Saitoh, N. Hayashi, and M. Yamamoto, eds., Int. Soc. Anal. Appl. Comput. 9, Kluwer Academic Publishers, Dordrecht, The Netherlands, 2001, pp. 87–103.
[15] V. Isakov, *On uniqueness and stability of the Cauchy problem*, Contemp. Math., 209 (1997), pp. 131–146.
[16] S. I. Kabanikhin and A. L. Karchevsky, *Optimizational method for solving the Cauchy problem for an elliptic equation*, J. Inverse Ill-Posed Probl., 3 (1995), pp. 21–46.
[17] M. V. Klibanov and F. Santosa, *A computational quasi-reversibility method for Cauchy problems for Laplace's equation*, SIAM J. Appl. Math., 51 (1991), pp. 1653–1675.
[18] R. Lattés and J.-L. Lions, *The Method of Quasi-Reversibility: Applications to Partial Differential Equations*, translated from the French and edited by R. Bellman, Elsevier, New York, 1969.
[19] M. M. Lavrent'ev, *On the Cauchy problem for the Laplace equation*, Izv. Akad. Nauk. SSSR Ser. Mat., 20 (1956), pp. 819–842.
[20] M. M. Lavrent'ev, V. G. Romanov, and S. P. Shishatskii, *Ill-Posed Problems of Mathematical Physics and Analysis*, Transl. Math. Monogr. 64, AMS, Providence, RI, 1986.
[21] A. Leitão, *An iterative method for solving elliptic Cauchy problems*, Numer. Funct. Anal. Optim., 21 (2000), pp. 715–742.
[22] J. L. Mueller and S. Siltanen, *Direct reconstructions of conductivities from boundary measurements*, SIAM J. Sci. Comput., 24 (2003), pp. 1232–1266.
[23] A. I. Nachman, *Reconstructions from boundary measurements*, Ann. Math., 128 (1988), pp. 531–576.
[24] J. Saranen and G. Vainikko, *Periodic Integral and Pseudodifferential Equations with Numerical Approximation*, Springer, Berlin, 2002.
[25] S. Siltanen, *Electrical Impedance Tomography and Faddeev's Green Function*, Ph.D. thesis, Helsinki University of Technology, Helsinki, Finland, 1999.
[26] S. Siltanen, J. Mueller, and D. Isaacson, *An implementation of the reconstruction algorithm of A. Nachman for the 2-D inverse conductivity problem*, Inverse Problems, 16 (2000), pp. 681–699.
[27] Z. Sun and G. Uhlmann, *Recovery of singularities for formally determined inverse problems*, Comm. Math. Phys., 153 (1993), pp. 431–445.
[28] J. Sylvester and G. Uhlmann, *Global uniqueness theorem for an inverse boundary value problem*, Ann. Math., 125 (1987), pp. 153–169.
[29] N. N. Tarkhanov, *The Cauchy Problem for Solutions of Elliptic Equations*, Math. Topics 17, Akademie Verlag, Berlin, 1995.
[30] A. N. Tikhonov, *Solution of incorrectly formulated problems and the regularization method*, Soviet Math. Dokl., 4 (1963), pp. 1035–1038.
[31] G. Uhlmann, *Developments in inverse problems since Calderón's foundational paper*, in Harmonic Analysis and Partial Differential Equations, M. Christ, C. E. Kenig, and C. Sadosky, eds., University of Chicago Press, Chicago, London, 1999, pp. 295–345.
[32] G. Vainikko, *Fast solvers of the Lippmann-Schwinger equation*, in Direct and Inverse Problems of Mathematical Physics (Newark, DE), Int. Soc. Anal. Appl. Comput. 5, R. P. Gilbert, J. Kajiwara, and Y. S. Xu, eds., Kluwer Academic Publishers, Dordrecht, The Netherlands, 2000, pp. 423–440.
[33] J. M. Varah, *A practical examination of some numerical methods for linear discrete ill-posed problems*, SIAM Rev., 21 (1979), pp. 100–111.
[34] Sh. Yarmukhamedov, *On the Cauchy problem for the Laplace equation*, Dokl. Akad. Nauk SSSR, 235 (1977), pp. 281–283 (in Russian).
[35] Sh. Yarmukhamedov, *Harmonic extension of continuous functions defined on a piece of the boundary*, Russian Acad. Sci. Dokl. Math., 46 (1993), pp. 430–434.
[36] Sh. Yarmukhamedov, *Integral representation of a CR-function and its holomorphic continuation*, Dokl. Math., 51 (1995), pp. 253–255.
[37] Sh. Yarmukhamedov, *Continuing solutions to the Helmholtz equation*, Dokl. Math., 56 (1997), pp. 887–890.